OPEN ACCESS Freely available online

PLoS one

Eeyarestatin 1 Interferes with Both Retrograde and Anterograde Intracellular Trafficking Pathways

Mina-Olga Aletrari[1], Craig McKibbin[2¤a], Helen Williams[3], Vidya Pawar[1¤b], Paola Pietroni[1], J. Michael Lord[1], Sabine L. Flitsch[3,4], Roger Whitehead[3], Eileithyia Swanton[2], Stephen High[2]*, Robert A. Spooner[1]*

1 School of Life Sciences, University of Warwick, Coventry, United Kingdom, **2** Faculty of Life Sciences, University of Manchester, Manchester, United Kingdom, **3** School of Chemistry, University of Manchester, Manchester, United Kingdom, **4** Manchester Interdisciplinary Biocentre, University of Manchester, Manchester, United Kingdom

Abstract

Background: The small molecule Eeyarestatin I (ESI) inhibits the endoplasmic reticulum (ER)-cytosol dislocation and subsequent degradation of ERAD (ER associated protein degradation) substrates. Toxins such as ricin and Shiga/Shiga-like toxins (SLTx) are endocytosed and trafficked to the ER. Their catalytic subunits are thought to utilise ERAD-like mechanisms to dislocate from the ER into the cytosol, where a proportion uncouples from the ERAD process, recovers a catalytic conformation and destroys their cellular targets. We therefore investigated ESI as a potential inhibitor of toxin dislocation.

Methodology and Principal Findings: Using cytotoxicity measurements, we found no role for ES_I as an inhibitor of toxin dislocation from the ER, but instead found that for SLTx, ESI treatment of cells was protective by reducing the rate of toxin delivery to the ER. Microscopy of the trafficking of labelled SLTx and its B chain (lacking the toxic A chain) showed a delay in its accumulation at a peri-nuclear location, confirmed to be the Golgi by examination of SLTx B chain metabolically labelled in the *trans*-Golgi cisternae. The drug also reduced the rate of endosomal trafficking of diphtheria toxin, which enters the cytosol from acidified endosomes, and delayed the Golgi-specific glycan modifications and eventual plasma membrane appearance of tsO45 VSV-G protein, a classical marker for anterograde trafficking.

Conclusions and Significance: ESI acts on one or more components that function during vesicular transport, whilst at least one retrograde trafficking pathway, that of ricin, remains unperturbed.

Citation: Aletrari M-O, McKibbin C, Williams H, Pawar V, Pietroni P, et al. (2011) Eeyarestatin 1 Interferes with Both Retrograde and Anterograde Intracellular Trafficking Pathways. PLoS ONE 6(7): e22713. doi:10.1371/journal.pone.0022713

Editor: David Holowka, Cornell University, United States of America

Received April 19, 2011; **Accepted** June 28, 2011; **Published** July 25, 2011

Copyright: © 2011 Aletrari et al. This is an open-access article distributed under the terms of the Creative Commons Attribution License, which permits unrestricted use, distribution, and reproduction in any medium, provided the original author and source are credited.

Funding: This work was supported by funding from the Biotechnology and Biological Sciences Research Council (Grant number BB/D005752/1) http://www.bbsrc.ac.uk/, the National Institutes of Health (Grant number 5U01AI65869-02) http://www.nih.gov/and the Wellcome Trust (Program Grant number 080566/Z/06/Z) http://www.wellcome.ac.uk/. The funders had no role in study design, data collection and analysis, decision to publish, or preparation of the manuscript.

Competing Interests: The authors have declared that no competing interests exist.

* E-mail: R.A.Spooner@warwick.ac.uk (RAS); stephen.high@manchester.ac.uk (SH)

¤a Current address: Department of Clinical Biochemistry, Royal Surrey County Hospital, Guildford, United Kingdom
¤b Current address: Institute of Cancer Research, Chester Beatty Laboratories, London, United Kingdom

Introduction

The plant toxin ricin and the bacterial Shiga and Shiga-like toxins (SLTx) bind their receptors (glycoproteins/glycolipids bearing exposed β1→4 linked galactose residues and the sphingolipid Gb3 respectively) at the mammalian cell surface and, after internalization by endocytosis, traffic in vesicular carriers to the endoplasmic reticulum (ER) [1] (Figure 1). Here, the toxic A chain (RTA) of ricin is reductively separated from its receptor-binding B chain (RTB) [2], [3] and then unfolds and partially inserts into the ER membrane [4]. This change in structure is thought to mimic a misfolded membrane-associated protein, allowing RTA to co-opt components of the ER-associated protein degradation (ERAD) pathways that remove misfolded proteins and orphan subunits from the ER in order to maintain ER homeostasis [5], [6], [7].

Typical soluble ERAD substrates are unfolded in the ER lumen and then extracted (dislocated) to the cytosol. During dislocation, substrates are usually polyubiquitylated on internal lysine residues by membrane integral E3 ubiquitin ligases such as HRD1. This process provides tags for the cytosolic AAA (ATPase associated with various cellular activities)-ATPase extraction motor p97/VCP [8], [9], [10] and subsequently, after limited de-ubiquitylation [11], [12], [13] for the proteasome [14], which is the terminal destination for ERAD substrates. RTA can be co-immunoprecipitated with the Sec61 translocon [15], which is a putative component of the dislocation machinery [16], and with EDEM, an ERAD-associated mannosidase [17]. Furthermore, RTA dislocation and cytotoxicity are sensitive to manipulation of expression levels of SEL1L [18], a regulator of the HRD complex. All these observations are consistent with use by RTA of endogenous ERAD components. Post-dislocation, cytosolic triage by molecular chaperones permits folding of a proportion of cytosolic RTA to an active conformation and therefore at least a fraction of dislocated RTA uncouples from the final ERAD step of proteasomal degradation [19]. Refolded cytosolic RTA then depurinates the large ribosomal subunit at one specific site [20], resulting in cessation of protein synthesis and ultimately in cell death. The RTA dislocation process in mammalian cells remains otherwise unmapped. However, when expressed in the ER of the

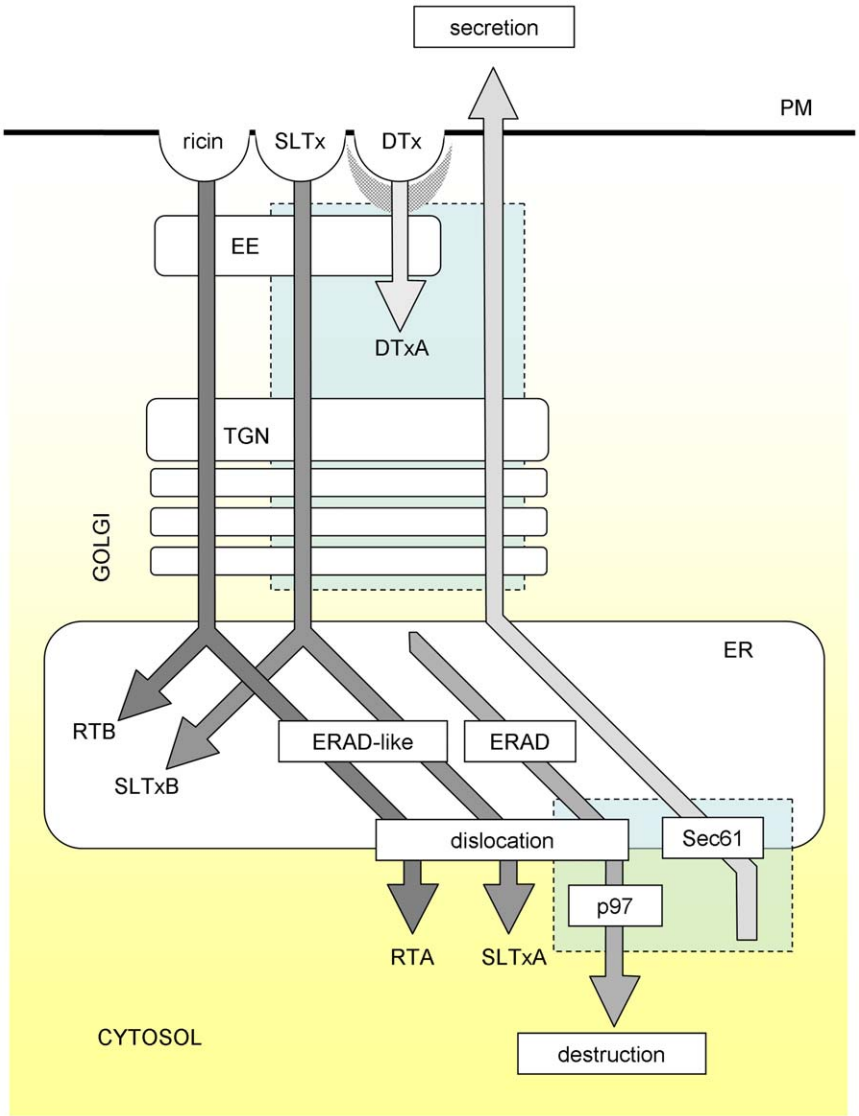

Figure 1. Vesicular trafficking schemes. Following clathrin-independent endocytosis, the cytotoxic fractions of ricin and Shiga –like toxin (SLTx) traffic to the ER *via* early endosmes (EE), the *trans*-Golgi network (TGN) and the Golgi apparatus to the endoplasmic reticulum (ER), where the ricin subunits RTA and RTB are reductively separated. It is assumed that SLTxA chain is also separated from its B chain pentamer (SLTxB) in the ER. The toxic RTA and SLTxA chains are thought to co-opt ERAD mechanisms to dislocate from the ER to the cytosol, where they are refolded to recover toxic catalytic activity (ribosome modification). Diphtheria toxin (DTx) is endocytosed in a clathrin-dependent manner (hatched area) and enters the cytosol from acidified endosomes. In the cytosol it is reduced, releasing the A chain (DTxA) which inactivates elongation factor 2. Blue boxes, areas/processes affected by ES_I: lower box, previously identified targets; upper box, this study. PM, plasma membrane.
doi:10.1371/journal.pone.0022713.g001

yeast *Saccharomyces cerevisiae*, RTA also utilizes components of the yeast equivalent of the mammalian HRD1 complex (the Hrd1p complex) for dislocation [21]. SLTx A chain (SLTxA) has identical catalytic activity to RTA [22], and the holotoxin traffics to the ER in a superficially similar manner to ricin [1] (Figure 1). It is widely assumed that SLTxA also utilizes ERAD components for dislocation to the cytosol. Little is known about the dislocation process for SLTxA, other than interactions with ER chaperones and Sec61 prior to dislocation [23], [24].

Mammalian major histocompatibility complex (MHC) Class I heavy chains are normally expressed as type I membrane proteins in the mammalian endoplasmic reticulum (ER), where they are chaperoned until assembly with their partner β-microglobulin chains [25], [26]. Each complex then binds a peptide derived from proteins degraded in the cytosol that enters the ER lumen via transporters associated with antigen processing (TAPs). The assembled complex is trafficked via secretory vesicle carriers to the plasma membrane, allowing peptide display to cells of the immune system [27]. The cytomegalovirus immunoevasin protein US11 down-regulates the expression of assembled complexes by stimulating dislocation of folded MHC Class I molecules from the ER to the cytosol. Here they are deglycosylated and then degraded by the proteasome [28]. US11 interacts with numerous components [29], [30] of the ER membrane integral HRD1 ubiquitylation complex which is responsible for polyubiquitylating the MHC Class I heavy chains during dislocation [31], [32]. This HRD complex is fully functional in the absence of US11, dislocating unassembled MHC Class I heavy chains [33] as well as other

ERAD substrates [5], [6]. The small molecule eeyarestatin I (ES_I) was identified in a high throughput screen for increased fluorescence of mammalian cells expressing both an enhanced green fluorescent protein (GFP)-Class I MHC heavy chain fusion and the US11 gene product. ES_I was subsequently shown to also inhibit ERAD of orphan T cell receptor α (TCRα) subunits in the absence of US11 [34]. The mechanism of ES_I action is not yet clear and the initial suggestion that it interfered with pre-dislocation steps [34] was followed by evidence of an effect on a post-dislocation step, namely p97-associated de-ubiquitylation [35], [36], [37], a perturbation of co-translational translocation at the ER, most likely through inhibition of Sec61 functions [38], and formation of cross-linked adducts in the ER lumen between protein disulphide isomerase (PDI) and an ERAD substrate [39].

The degradation of ERAD substrates normally requires both ER dislocation and p97 activities, and since ES_I has been reported to perturb both processes [34], [35], [38], we investigated its effects on the cytotoxicity of ER-trafficking toxins. We report here that the later stages of the cytotoxic process for two toxins, ricin and SLTx, are unaffected by ES_I treatment (see Figure 1). This suggests that in both cases the dislocation of their respective toxic A chains across the ER membrane, and their subsequent delivery into the cytosol, is unperturbed by the compound. However, we find that SLTx toxicity is specifically reduced by ES_I treatment. We show that this effect results from interference with a much earlier stage of the cytotoxic process, resulting in a delay in the delivery of the holotoxin to the ER. Further studies revealed that ES_I can interfere with both the anterograde and retrograde transport of vesicular cargoes through the endomembrane system and we conclude that the ES_I is most likely capable of perturbing multiple cellular targets.

Results

ES_I treatment protects HeLa cells from challenge with SLTx but not ricin

The toxic A chains of ricin and SLTx have identical RNA *N*-glycosidase activities, removing a single adenine residue from the large ribosomal subunit at the site of interaction with elongation factor complexes [20], [22], resulting in a cessation of protein synthesis. Cytotoxicity can therefore be determined by comparing the remaining levels of *de novo* protein synthesis capability in toxin-challenged cells to those in non-toxin treated cells by pulsing toxin-treated and control cells with radiolabelled amino-acids and measuring their incorporation into acid-precipitable material (proteins). HeLa cells were pretreated with ES_I or its inactive derivative ES_{R35} [38] for 1 h and then challenged for 1, 2 or 4 h with dilutions of ricin or SLTx in medium containing ES_I or ES_{R35} as appropriate, such that the compounds were present throughout the toxin challenge period (see Methods). Remaining protein synthesis at each toxin dilution was normalized to that of drug-treated, but non-toxin treated, controls. For each individual experiment a coeval control was performed, substituting DMSO (the vehicle in which ES_I and ES_{R35} were dissolved) for ES_I or ES_{R35}, and here protein synthesis levels were normalized to DMSO-treated, but not toxin-treated, controls. ES_I treatment alone had some toxicity in this assay, since it reduced the protein synthesis ability of the cells (Figure 2A), but it had no obvious effect on the cytotoxicity of ricin (Figure 2B). In contrast, ES_I treatment protected cells ~2.5 fold from challenge with SLTx (Figures 2C, D). ES_{R35} had little or no effect in any of these assays.

These results initially suggested a mechanistic difference in the ER to cytosol dislocation of RTA and SLTxA. ES_I perturbs the mammalian ubiquitin proteasome system (UPS) [35], so we examined the role of the proteasome in SLTx cytotoxicity to investigate whether this underlies its protective effect against SLTx but not ricin whose A chain dislocates independently of the UPS [21]. HeLa cells were challenged with SLTx in the presence of clasto-Lactacystin β-lactone (cLβ-l), an irreversible inhibitor of the three proteolytic activities of the proteasome [40]. However, despite a previous report that cLβ-l sensitizes Vero cells slightly to SLTx challenge [41], we saw no obvious effect in HeLa cells (Figure 3A). The effectiveness of cLβ-l was confirmed *in vitro*, by its inhibition of proteasomal degradation of casein (Figure 3B). Although the lack of obvious role for the proteasome in SLTx toxicity to HeLa cells may reflect a cell-type specific difference in the cytosolic fate of SLTxA, it should be noted that the previously reported effect of cLβ-l on SLTx cytotoxity was rather modest [41]. Our results suggest that the cytotoxicity of SLTxA is not strongly influenced by the UPS, and the protective effect of ES_I is most likely upstream of this process.

The mechanism of ES_I -dependent protection against SLTx was investigated further by examining the temporal profile of SLTx intoxication. HeLa cells were treated with a saturating dose of toxin (1 $\mu g.ml^{-1}$) for increasing lengths of time and the remaining ability of the cells to synthesise proteins was measured. In such experiments, there is a distinct lag before the first measurable loss of protein synthesis ability, followed by a reduction in total cell population protein synthesis ability whose (log) slope is determined by the dislocation rate [42], [43]. If ES_I reduces SLTxA dislocation, this would be measurable by a reduction in the log slope of the exponential phase, but the pre-cytosolic phase (lag) should be unaltered. We found little or no difference in the half-time ($T_{1/2}$, the time taken to reduce remaining protein synthesis ability by 50%) of the exponential phase. Strikingly, however, we measured instead a distinct intoxication lag phase increase of ~20 minutes for ES_I treatment, whilst ES_{R35} had no measurable effects in these experiments (Figure 3C, D). This observation suggests that the step affected by ES_I most likely involves the delivery of the toxin to the ER, and is hence upstream of dislocation (see Figure 1).

ES_I treatment perturbs SLTx trafficking

To examine whether ESI treatment delays delivery of SLTx to the ER, we applied fluorescently-labeled SLTx B chain pentamer (SLTxB) or holotoxin to HeLa cells, and followed its intracellular transport by confocal microscopy. Endocytosed recombinant SLTxB traffics to the ER in the same way as SLTx holotoxin, *via* early endosomes (EE), the *trans*-Golgi network (TGN) and the Golgi stack to the ER [44]. In control cells treated with DMSO or ES_{R35}, fluorescently-labeled SLTxB (Cy3-SLTxB) accumulated at a juxta-nuclear position within 40 minutes in those cells that had taken up visible amounts of SLTxB (Figure 4A, Cy3-SLTxB), an accumulation that has been previously shown to occur in the TGN and the Golgi stack [45], [46]. In contrast, in ES_I treated cells, SLTxB was not observed in this location until 60 minutes following application, showing a delay in the retrograde trafficking of the toxin B chain. The same qualitative delay was also evident when these experiments were repeated using fluorescently labeled SLTx holotoxin (Figure 4A, Cy2-SLTx).

To define this delay biochemically we used SLTxB-$(Sulf)_2$ [46], a recombinant SLTxB chain pentamer whose subunits bear a C-terminal tag that can be radiolabelled with [^{35}S]-sulfate upon entry to the *trans*-Golgi cisternae [47]. Relative to control cells treated with DMSO, in ES_I -treated cells an initial delay in [^{35}S]-labeling of SLTxB-$(Sulf)_2$ was observed, indicating delayed entry of SLTxB-$(Sulf)_2$ to the *trans*-Golgi cisternae. This was followed by saturated labeling, suggesting a longer residence of the SLTxB-$(Sulf)_2$ pentamer in these cisternae upon ES_I treatment (Figure 4B,

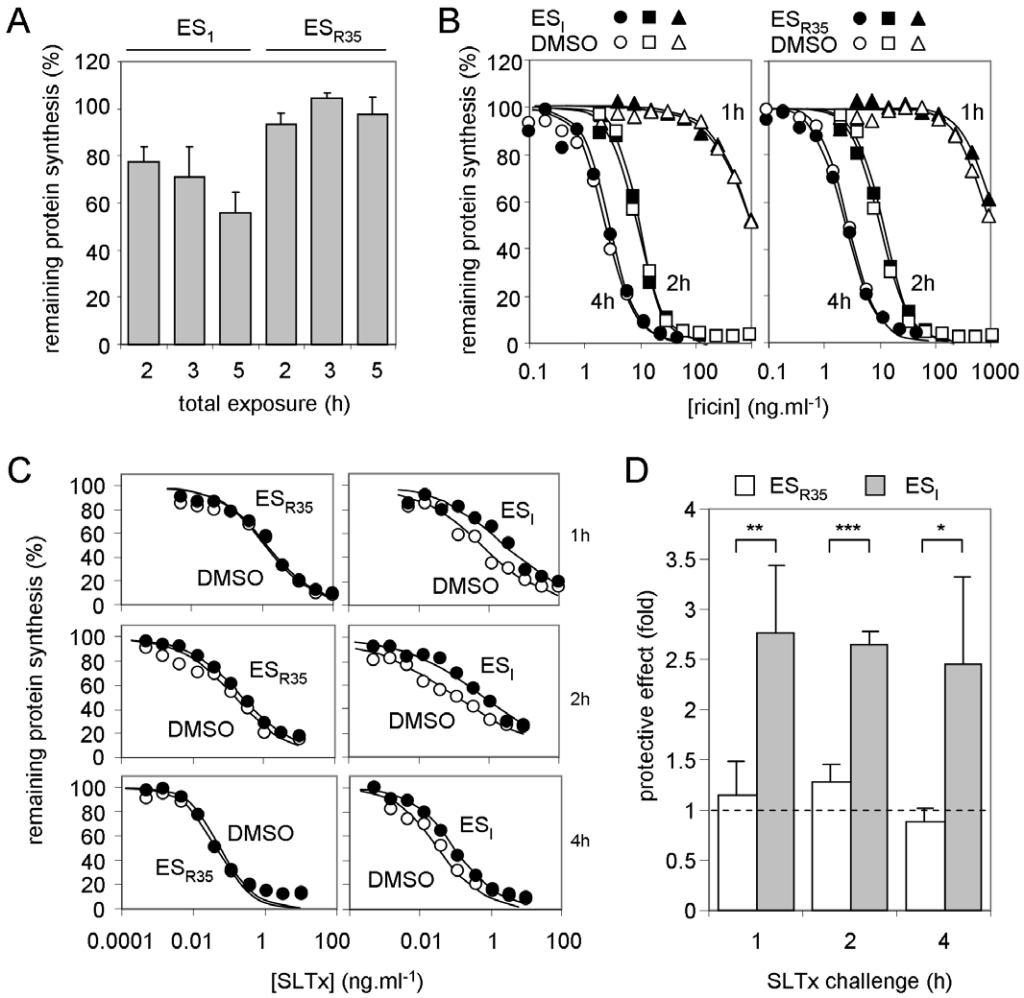

Figure 2. ES_I treatment protects HeLa cells from SLTx, but not from ricin. A. ES_I treatment reduces cellular protein synthesis levels. Cells were treated with ES_I or its inactive derivative ES_{R35} for 2, 3 or 5 h, and remaining protein synthesis ability was determined, shown relative to control cells treated with the vehicle DMSO. N = 3, bars +/− 1 S.D. **B. ES_I treatment has no effect on ricin intoxication.** Cells treated with DMSO (open symbols), ES_I (filled symbols, left-hand panel) or ES_{R35} (filled symbols, right hand panel) were challenged for 1 (circles), 2 (squares) or 4 h (triangles) with graded doses of ricin and remaining protein synthesis levels were determined. Typical single assays are shown. **C, D. ES_I treatment protects cells from SLTx challenge.** Cells treated with DMSO, ES_I or ES_{R35} were challenged with graded doses of SLTx for 1 (upper), 2 (middle) or 4 h (lower) and remaining levels of protein synthesis ability were determined. Typical single assays are shown in **C**, from which the IC_{50} (concentration of SLTx that reduced protein synthesis to half that of control non-toxin treated cells treated in parallel) values were determined, and means of 3 or 4 independent experiments (+/− 1 S.D.) are shown in **D**, expressed as fold protection (IC_{50} drug treated cells: IC_{50} DMSO treated cells). Protective effects from ES_I and ES_{R35} treated cells were compared using an unpaired t-test (1 h, p = 0.0048, t = 4.358, n = 4; 2 h, p<.0001, t = 12.28, n = 4; 4 h, p = 0.0377, t = 3.060, n = 3; *, significant: **, very significant: ***, extremely significant).
doi:10.1371/journal.pone.0022713.g002

C). On the basis of these results, we conclude that both SLTx entry to the *trans*-Golgi cisternae and subsequent egress from this location are both inhibited by ES_I treatment of cells.

ES_I treatment protects cells from diphtheria toxin challenge

SLTx is delivered to the *trans*-Golgi cisternae from an EE compartment via the TGN [1], and therefore the temporal delay in Golgi arrival might reflect reduced rates of trafficking at the endosomal level. In contrast to ER trafficking toxins, following endocytosis diphtheria toxin (DTx) translocates across the endosomal membrane to enter the cytosol as the endosomal pH drops to ≤5.3 (Figure 1) [48]. Strikingly, we found that ES_I treatment protected cells from DTx, particularly for shorter intoxication times (Figure 5A, B). In contrast, ES_{R35} had no effect for short intoxications, and may even have had a slight sensitizing effect for longer toxin challenges (Figure 5A, B). The protective effect of ES_I again correlated with an increased lag prior to cytosolic delivery of the toxin subunit, with little or no difference measured in the toxin translocation rate (Figure 5C, D).

ES_I treatment delays anterograde trafficking of tsO45VSV-G-GFP from the ER

The retrograde trafficking defects resulting from ES_I treatment do not reflect a pleiotropic effect on all aspects of vesicular transport, since the compound has no measureable effect on ricin cytotoxicity (Figure 2B). To investigate further the effects of ES_I on vesicular trafficking, we examined anterograde transport in ES_I-treated cells.

The mutant vesicular stomatitis virus glycoprotein tsO45 VSV-G exhibits temperature sensitive transport from the ER to the cell

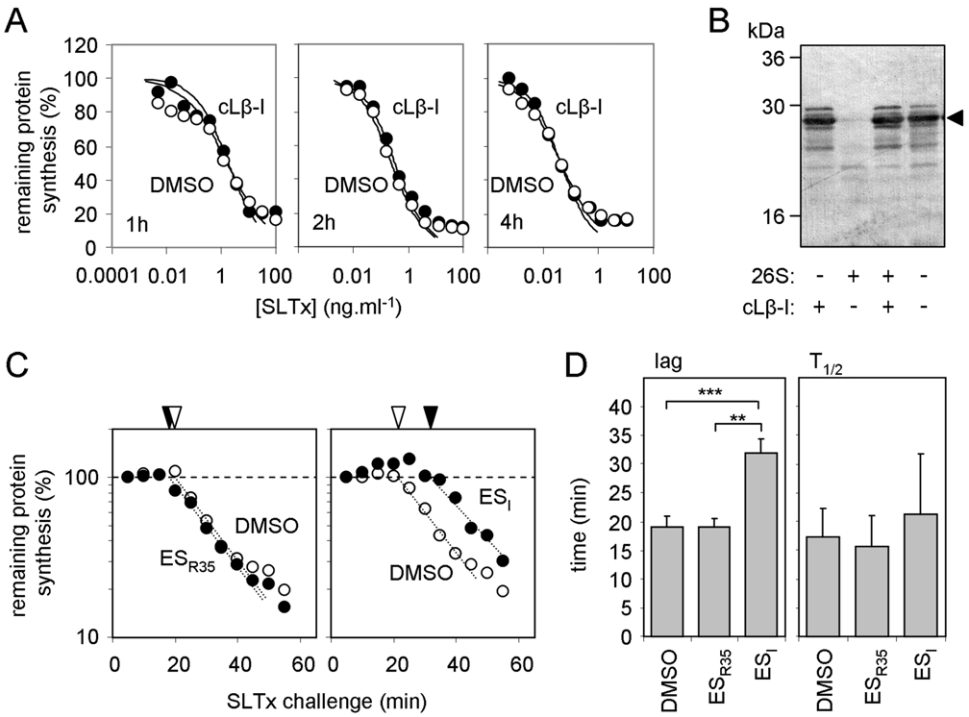

Figure 3. ES_I causes a delay in intoxication of HeLa cells with SLTx. A, B. The UPS has little influence on SLTx cytotoxicity. A. Cells treated with the proteasome inhibitor *clasto* Lactacystin β-lactone (cLβ-I) were challenged with SLTx for 1 (left), 2 (middle) or 4 h (right) and remaining levels of protein synthesis were determined. **B.** Efficacy of cLβ-I was confirmed *in vitro* by its ability to block degradation of casein (arrowhead) in the presence of mammalian 26S proteasomes. **C.** Cells treated with ES_{R35} (left hand panel) or ES_I (right hand panel) were challenged with a fixed dose (1 $\mu g.ml^{-1}$) of SLTx for increasing periods and protein synthesis levels were determined. Exponential fits (dotted lines) were extrapolated to determine the lag phase of intoxication (white arrowhead, DMSO; black arrowhead, drug). Typical single assays are shown. **D.** Lag phases were determined as in **C**, and the half-lives of protein synthesis ($T_{1/2}$) were determined from exponential fits in **C.** DMSO, n = 6, +/− 1.S.D., ES_I and ES_{R35}, n = 3, +/− 1 S.D. Values were compared using unpaired t-tests. Lags: DMSO *versus* ES_{R35}, no significant difference; DMSO versus ES_I, $p<0.0001$, $t = 8.347$; ES_I versus ES_{R35} $p = 0.0016$, $t = 7.658$; **, very significant: ***, extremely significant. $T_{1/2}$ values: no significant differences.
doi:10.1371/journal.pone.0022713.g003

surface [49] and has become a classical marker for transit through the secretory pathway [50]. At the restrictive temperature (40°C), the protein is misfolded and cycles between the ER, the ER-Golgi intermediate compartment (ERGIC) and the *cis*-Golgi network. However, after a shift to the permissive temperature (32°C), it is released from this cycle and is efficiently trafficked to the cell surface [51]. This system provides an ideal platform from which to investigate the effect of ES_I on anterograde transport, independently of any effects of the drug on protein synthesis (Figure 2A) or on membrane integration [38].

Cells were infected with adenovirus encoding a GFP-tagged tsO45 VSV-G (tsO45 VSV-G –GFP) and grown overnight at 40°C. Upon a temperature shift from 40°C to 32°C, tsO45 VSV-G-GFP was released from the early secretory pathway, accumulating in a peri-nuclear region by ~30 min and appearing primarily at the cell surface after 1 to 2 hours in cells incubated with DMSO or ES_{R35} (Figure 6A, DMSO and ES_{R35} panels). In contrast, when cells were treated with the fungal metabolite Brefeldin A (BFA), which blocks secretion by stimulating Golgi and ER membrane fusion [52], [53], [54], tsO45 VSV-G-GFP remained within the fused ER-Golgi compartment following the temperature shift and did not reach the cell surface even after 2 hours (Figure 6A, BFA panels). In most ES_I treated cells, the bulk of the tsO45 VSV-G-GFP protein remained at an intracellular location even after 2 hours, although some degree of cell surface labeling was apparent at both 1 and 2 hours (Figure 6A, ES_I panels).

To underpin this microscopy-based analysis of VSV-G trafficking, we also examined Golgi-dependent alterations in the *N*-linked glycans of the VSV-G protein to investigate its progress through the secretory pathway. During passage through the Golgi, the *N*-linked glycans of VSV-G are modified such that they acquire resistance to in vitro removal by the enzyme endoglycoside H (EndoH) [55]. In lysates of HeLa cells expressing tsO45 VSV-G, ES_I treatment delayed the conversion of the glycoprotein into an EndoH-resistant form, such that even after 2 hours a population of EndoH-sensitive glycoprotein was still present (Figure 6B, compare ES_I with DMSO and ES_{R35}). In the case of BFA, we noted a more rapid acquisition of EndoH resistance (Figure 6B, BFA) consistent with the entry of Golgi α-mannosidase II (whose activity converts *N*-glycans from EndoH sensitivity to resistance) into the ER upon BFA treatment [56]. Taken together, these data indicate that the anterograde trafficking of VSV-G through the secretory pathway, and its appearance at the cell surface, are delayed by ES_I treatment.

Finally, we examined the effects of ES_I on the morphology of organelles used by intracellular trafficking toxins. Typically, long drug pretreatments (8–48 h) have been used in experiments that demonstrate efficacy of ES_I- in retarding the dislocation of an ERAD substrate [34], inhibition of p97-associated functions [35], and linkage of ER stress with activation of the ATF3 and ATF4 transcription factors [57]. However, even with exposures as short as 1 hour, ES_I exhibits biological activity, with clear effects on protein translocation into the ER [38]. Immunofluorescence

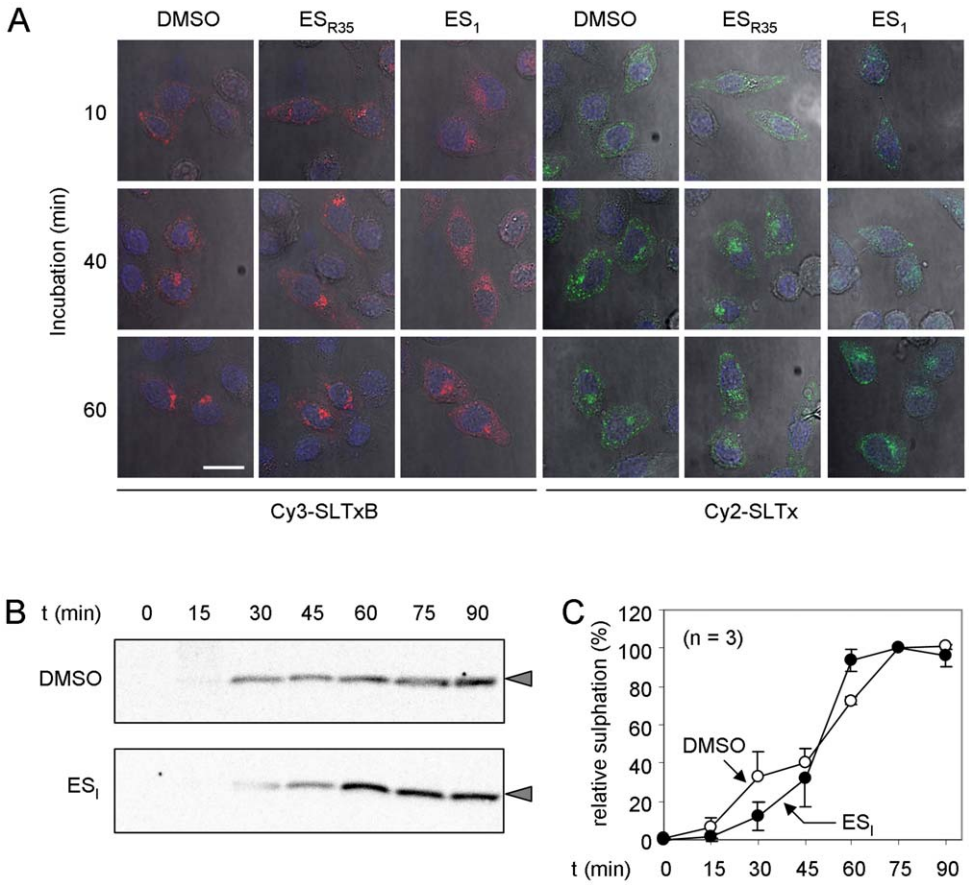

Figure 4. ES$_I$ treatment interferes with retrograde trafficking of SLTx. A. Cells were treated with DMSO, ES$_I$ or ES$_{R35}$ and then incubated for increasing periods with Cy3-labelled SLTxB (red) or Cy2-labelled SLTx (green), after which they were fixed and examined by confocal microscopy. Blue, DAPI-stained nuclei, white scale bar, 25 μm. **B.** Cells starved of sulphate were incubated with [^{35}S]O$_4$, treated with DMSO or ES$_I$ and then incubated for increasing periods with a modified recombinant SLTxB pentamer, whose monomers bear a sulphation motif that is sulphated in the *trans*-Golgi cisternae. SLTxB-sulf (arrowheads) was immunoprecipitated from detergent lysates of the cells and revealed after SDS-PAGE by fluorography and autoradiography. **C.** Relative sulphation of SLTxB-sulf, determined from experiments performed in **B**, n = 3, +/− 1 S.D.
doi:10.1371/journal.pone.0022713.g004

microscopy revealed that 8 h treatment with ES$_I$ resulted in extensive vacuolation of the ER consistent with pathological effects resulting from ER stress [58]. In contrast, there were no obvious effects on lysosomal and Golgi morphology (Figure S1). Importantly, the effects of ES$_I$ treatment on the cytotoxicity of ER-dislocating toxins shown here were performed at shorter time intervals, specifically before any overt changes in cellular morphology were apparent (data not shown).

Discussion

We show that ES$_I$ interferes with both anterograde and retrograde transport of vesicular cargoes. Although no obvious morphological changes to Golgi structure were seen even after extended (8 hour) treatments of HeLa cells with ES$_I$, we detected a clear delay in the trafficking of VSV-G protein through the Golgi and its subsequent appearance at the cell surface. The nature of the VSV-G trafficking assay allows us to ascribe this as an effect on vesicular transport, and this effect is consistent with our previous observation that ES$_I$ treatment almost completely inhibits the secretion of newly synthesized proteins from HepG2 cells [38]. When taken together with the data presented here, we conclude that the strong ES$_I$ dependent inhibition of protein secretion that we previously observed is most likely due to multiple effects, with the drug reducing rates of protein synthesis (this study), affecting Sec61-mediated translocation across the ER membrane [38] and delaying subsequent vesicular transport to the cell surface (this study).

ES$_I$ treatment was also found to inhibit the retrograde transport of DTx to low pH endosomes. The initial stages of DTx uptake rely on the endocytic pathway of the host cell, and our data indicate that the effects of ES$_I$ with respect to DTx are at this early stage of the process and not at the later membrane translocation step (Figure 1).

In addition, ES$_I$ treatment inhibits the retrograde transport of SLTx to and through the Golgi stack. Strikingly however, there was no measurable affect on the cytotoxicity of ricin, which, like SLTx, is thought to traffic via EE, the TGN and Golgi to the ER (Figure 1). Despite the superficial similarities in retrograde trafficking of ricin and SLTx, there are a number of characterized differences, particularly during transit through the Golgi. Hence, SLTx traverses the Golgi in a Rab6A'-dependent manner [59], [60], [61], whilst ricin traffics through the Golgi in a Rab6A'-independent manner [62]. Other differences include the strong inhibition of SLTx trafficking but weak inhibition of ricin trafficking by knockdown of syntaxin 5 [63] and the different requirements for sorting nexins at the endosome-TGN interface [64], [65], [66], [67]. Thus ES$_I$ does not act as a general inhibitor

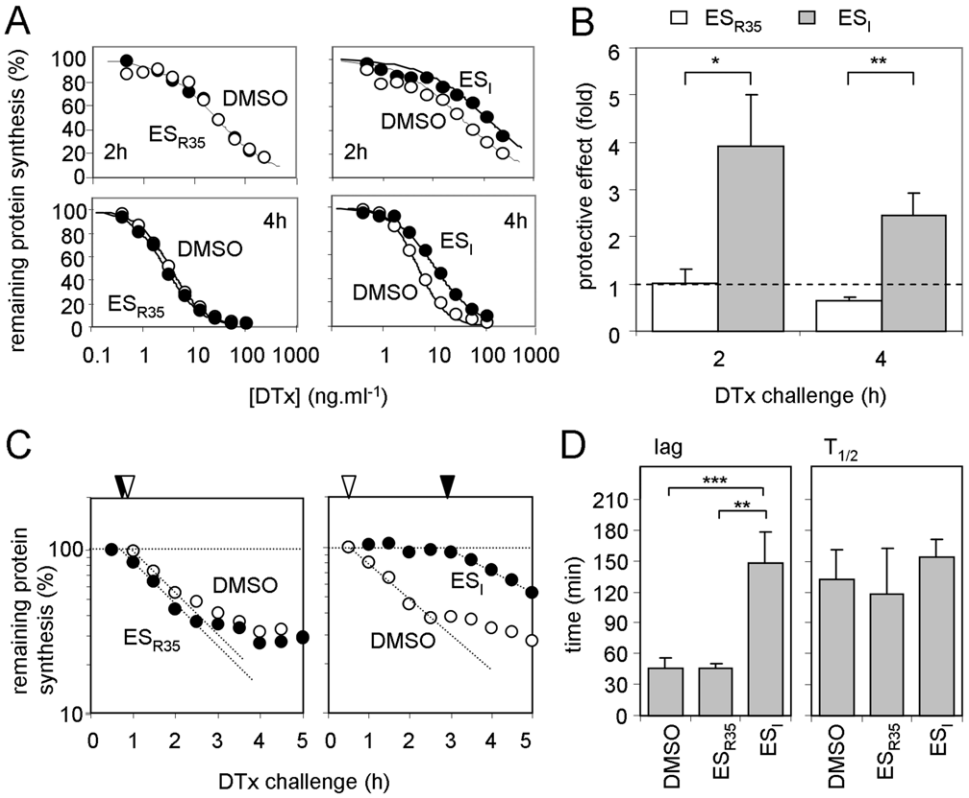

Figure 5. ES_I treatment protects cells from DTx challenge. A. Typical single cytotoxicity profiles of DMSO, ES_I and ES_{R35} treated HeLa cells subsequently challenged with graded doses of DTx for 2 (upper) or 4 h (lower). **B.** Protective effect of the drugs, determined from assays in **A**. n = 3, +/− 1.S.D. Protective effects from ES_I and ES_{R35} treated cells were compared using an unpaired t-test (2 h, p = 0.0104, t = 4.555; 4 h, p = .00024, t = 6.858; *, significant: **, very significant). **C.** Typical single assays showing the temporal profile of DTx cytotoxicity to cells treated with DMSO, ES_I or ES_{R35}, and determination of the lag phase (dotted lines and arrowheads, coded as in Figure 3C). **D.** Lag phases and half-lives of protein synthesis ($T_{1/2}$) were determined. DMSO, n = 6, +/− 1.S.D., ES_I and ES_{R35}, n = 3, +/− 1 S.D. Values were compared using unpaired t-tests. Lags: DMSO *versus* ES_{R35}, no significant difference; DMSO versus ES_I, $p<0.0001$, t = 8.810; ES_I versus ES_{R35} p = 0.0028, t = 6.573; **, very significant: ***, extremely significant. $T_{1/2}$ values: no significant differences.
doi:10.1371/journal.pone.0022713.g005

of vesicular trafficking, since at least one retrograde pathway is unresponsive to treatment (see Figure 1). The substrate specificity of ES_I inhibition further underlines that there are multiple routes or mechanisms by which exogenous toxins can reach the ER by retrograde transport [68], [1].

ES_I is unlikely to inhibit toxin action directly, since DTx and SLTxA1 have different targets and mechanisms of action (elongation factor-2 modification and ribosome modification, respectively), and the rate of intoxication after the initial lag phase is unaltered for both of these toxins. We cannot formally exclude the possibility that one or more of the currently suggested modes of action of ES_I, namely interference with early dislocation [34], p97-associated [12], [35] or ER translocation processes [38], results in the selective inhibition of specific intracellular trafficking routes. However, we found no effect of ES_I treatment upon the kinetics of dislocation of any of the toxins that we investigated in this study. In the case of RTA and SLTxA, this suggests that the ER-cytosol dislocation of both of these toxins does not involve the early ES_I inhibited step identified by Fiebiger and colleagues [34], or either of the two proposed targets of ESI: p97 and the Sec61 translocon [12], [35], [38]. A recent report noted ES_I-induced cross-links between PDI and an ERAD substrate [39]. PDI is thought to be responsible for the reductive cleavage of ricin, releasing RTA chain from its RTB partner in the ER lumen, a necessary prerequisite for the ER dislocation of the A chain [2], [3]. Since ES_I had no effect on the cytotoxicity of ricin, it seems unlikely that it induced cross-links between RTA and PDI over the short time scales used for cytotoxicity measurements. However, it should be noted that the inhibitory effect of ES_I when applied to intact cells is incomplete [38]. Thus it is also conceivable that these previously defined steps or components are perturbed by ES_I, but that they are not rate-limiting for toxin dislocation across the ER membrane.

ES_I has a bi-modular structure, with a comparatively hydrophobic portion that acts as a membrane binding domain [36] and a 5-nitrofuran containing group that is required for its effects on protein secretion and ER translocation [38], as well as p97 function [36]. ES_{R35}, which lacks the nitrofuran group of ES_I, was ineffective in all of our assays. A number of studies have shown that 5-nitrofuran containing compounds cause diverse effects in biological systems including the inhibition of *Salmonella* growth [69] and topisomerase function [70] and the induction of oxidative stress [71]. Given these wide-ranging effects and the capacity of nitrofurans to undergo *in vivo* modifications [72], we conclude that the most likely explanation of our data is that ES_I acts on one or more currently unidentified components that function during vesicular transport. The siRNA-mediated perturbation of signal recognition particle-dependent protein targeting to the Sec61 translocon has been shown to result in selective defects in post-ER membrane trafficking [73]. Hence the ES_I dependent inhibition of

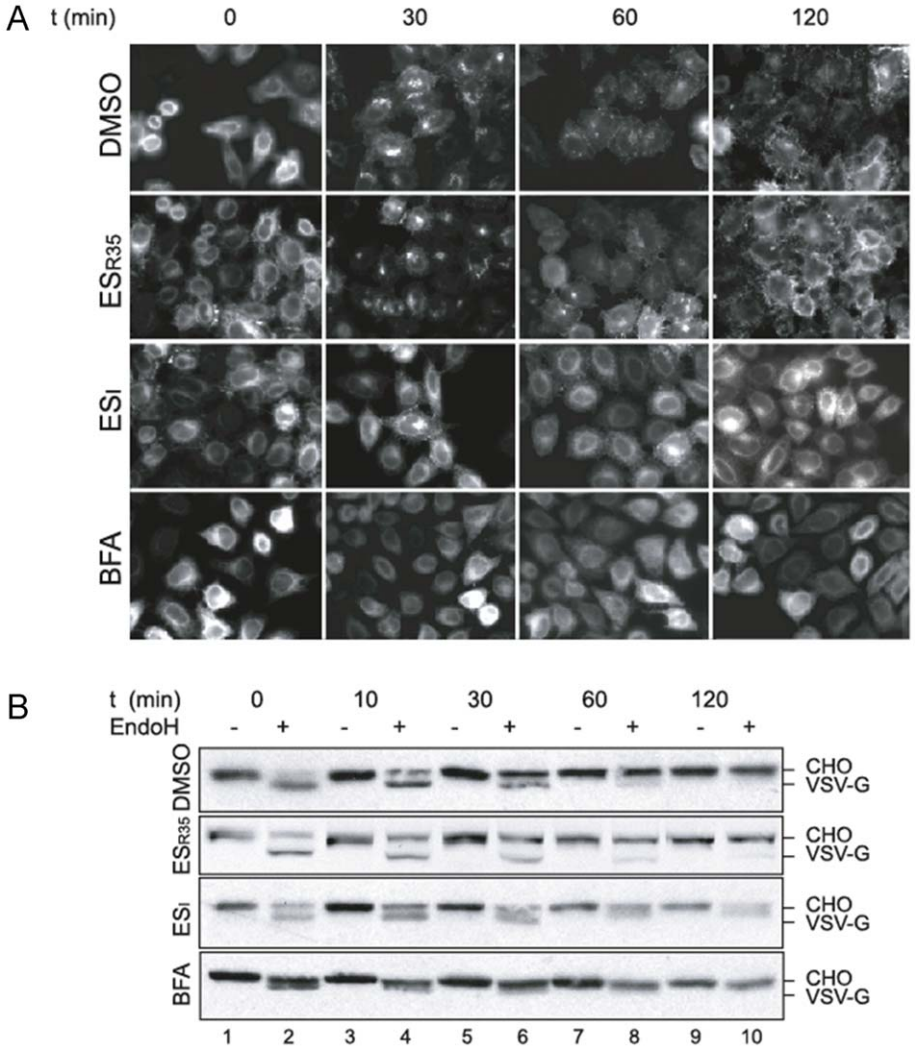

Figure 6. ES_I delays anterograde trafficking of tsO45 VSV-G-GFP. A. HeLa cells infected with adenovirus encoding tsO45 VSV-G-GFP were grown overnight at 40°C, then pre-treated with DMSO, with 8 μM ES_{R35}, ES_I, or with 5 $\mu g.ml^{-1}$ Brefeldin A (BFA) for 1 h. Cells were then shifted to 32°C, and incubated for the time indicated in the continued presence of the compounds, prior to fixation and visualisation by fluorescence microscopy. **B.** Lysates of HeLa cells treated as in **A** were incubated with Endoglycosidase H (EndoH, +) or mock treated (−), then analysed by SDS-PAGE followed by immunoblotting using anti-VSVG antibody and alkaline phosphatase conjugated secondary antibody. The position of *N*-glycosylated (CHO) and non-glycosylated VSV-G are indicated.
doi:10.1371/journal.pone.0022713.g006

Sec61 mediated translocation [38] could potentially contribute to the effects that we report here. However, as we saw an inhibitory effect within comparatively short timescales we believe it is more likely that components involved in vesicular trafficking are affected directly by ES_I, rather than being depleted as a consequence of any reduction in their synthesis or Sec61 mediated translocation. Given the inhibitory effect of ES_I upon p97-associated de-ubiquitylation [35], [36], [37], one possibility is that the compound may also impact one or more of the deubiquitinases implicated in endocytosis [74].

In the original study by Fiebiger et al., [34] the authors found that ES_I inhibits both the human cytomegalovirus protein US11-dependent degradation of MHC class I molecules, and the US11-independent degradation of TCRα, a well-defined model for a cellular ERAD substrate. The authors concluded that ES_I inhibits one or more stages just prior to, or concomitant with, dislocation from the ER. Given that a number of ERAD substrates appear to cycle between the ER and Golgi as a pre-requisite for subsequent dislocation [75], [76], [77], [21], and evidence of cross-talk between the secretory and ER degradative pathways [78], our new data raise the possibility that a perturbation of vesicular transport by ES_I may also contribute to the drug's inhibition of ER associated protein degradation.

Materials and Methods

Cell culture

HeLa cells that reliably express the SLTx receptor Gb3 [47] were used for all the cytotoxicity and SLTx trafficking experiments. HeLa cells used for the VSV-G assays and the data shown in Figure S1 were obtained from ATCC (CCL-2™). Cells were maintained in Dulbecco's modified Eagle's medium (DMEM) supplemented with 10% fetal calf serum (DMEM/FCS), and grown at 37°C in a 5% CO_2 atmosphere.

Cytotoxicity experiments

Cytotoxicity experiments were performed on cells seeded at 2×10^4 cells per well of a 96-well plate after overnight growth. Growth medium was replaced by DMEM/FCS containing drug (4 μM, from a stock dissolved in DMSO) or vehicle for 1 h. After this pretreatment, the medium was replaced by serial dilutions of toxin in DMEM/FCS containing either drug or vehicle as appropriate, and after incubation (see Figures for toxin incubation periods), the cells were rinsed in phosphate buffered saline, pH 7.4 (PBS) and incubated for 15 minutes in PBS containing 1 μCi.ml-1 [^{35}S]-methionine/cysteine (Perkin Elmer). Wells were then rinsed in PBS, and washed 5 times with cold 5% trichloroacetic acid. After addition of 200 μl Optiphase supermix scintillant (Perkin Elmer) to each drained well, and incubation at room temperature (~2 h), radioactivity incorporated into acid-precipitable material was determined by scintillation counting in a 1450 MicroBeta Trilux scintillation counter (Perkin Elmer). In all cases, toxin titration experiments for drug and vehicle were performed at the same time on the same 96-well plate, to remove any differences between plates. Data were normalized to coeval controls (nontoxin treated cells pretreated and treated with drug or vehicle treated as appropriate) and represent remaining protein synthesis (%). Concentrations (IC_{50}) of toxin that reduced protein synthesis ability to 50% were determined using a median effect plot [79], and protective effects were calculated as the ratio of IC_{50} drug:IC_{50} vehicle. For time course cytotoxicity experiments, cells were treated with a fixed concentration (1 $\mu g.ml^{-1}$) of toxin for increasing times (see Figures for details), but were otherwise treated as above.

Microscopy

HeLa cells seeded at 2×10^5 cells/well in 1 ml complete DMEM/FCS were grown overnight on methanol-sterilised coverslips in 12-well plates. They were then pre-treated with 0.1% DMSO, 4 μM ES_I or 4 μM ES_{R35} for 1 hour and then incubated in 250 μl ice-cold PBS (containing DMSO, ES_I or ES_{R35} as appropriate) and incubated with either Cy2-SLTx or Cy3-SLTxB for 30 minutes at 4°C. The PBS was then replaced with 1 ml of complete DMEM/FCS and incubated at 37°C and cells were fixed using 4% paraformaldehyde (PFA) as part of a time-course. The final time-point was fixed with 4% PFA at 37°C for 20 minutes. Following fixing, PFA was quenched using 30 mM glycine for 5 minutes and washed three times in PBS before mounting using Vectashield mounting medium containing DAPI (Vector Labs, Burlinghame, CA).

HeLa cells exposed to both Cy2-SLTx and Cy3-SLTxB were imaged sequentially using Leica SP5 confocal microscopy. Cells treated with Cy3-SLTx were imaged using the DPSS 561 laser with an emission bandwidth between 566 nm to 790 nm (red) and the 405 diode ultraviolet (UV) laser with an emission bandwidth between 381 nm to 477 nm to image the nuclei (blue). The argon laser (at 20%) was used to collect differential interface contrast (DIC) images using the 488 nm laser. Cells treated with Cy2-SLTxB were imaged using the argon laser (at 20%) utilizing the 488 nm laser with an emission bandwidth between 497 nm to 638 nm (green), also used to collect DIC images. Again the 405 diode UV laser with an emission bandwidth between 414 nm to 488 nm was used to image the nuclei (blue).

GFP-tagged VSV-G trafficking

HeLa cells seeded at 3×10^5 cells/well in 2 ml complete DMEM/FCS were grown overnight on methanol-sterilised coverslips in 6-well plates and infected with adenovirus. Encoding a GFP-tagged tsO45 VSV-G protein as described by Chui et al [80]. Post-infection, the medium was replaced with fresh DMEM/FCS and the cells were kept at 40°C overnight. The following day, cells were pretreated for 1 h at 40°C in fresh carbonate free medium containing DMSO (vehicle control), 8 μM ES_I, 8 μM ES_{R35} or 5 $\mu g.ml^{-1}$ Brefeldin A as appropriate. The cells were then shifted to the permissive temperature (32°C) and were fixed as above after various lengths of incubation (see appropriate Figure legends). Cells were mounted in Mowiol and imaged using an Olympus BX60 upright microscope and Metamorph software (Universal Imaging Corp.). Alternatively cells wre harvested in Triton IP buffer (10 mM Tris-HCl pH 7.6, 140 mM NaCl, I mM EDTA, 1% Triton x-100) and after a brief spin, the post-nuclear supernatant. was split into two aliquots. One aliquot was incubated overnight with 6670 $U.ml^{-1}$ of Endoglycosidase H as directed by the supplier (New England Biolabs). Samples were analysed by SDS-PAGE and immunoblotting with mouse anti-VSV-G antibody followed by alkaline phospatase conjugated anti-mouse-antibodiy (both from Sigma) and visualized by development with BCIP/NBT colour development substrate (Promega).

SLTx and SLTxB labeling with Cy dyes

Purified SLTx and SLTxB were labeled according to the manufacturer's instructions (GE Healthcare).

SLTxB sulfation assay

Cells were seeded at 10^6 per well in six-well plates, grown overnight and washed twice in sulfate-free DMEM (Gibco) lacking FCS. They were then incubated for 3 h, 37°C in sulfate-free medium lacking FCS in the presence of 200 $\mu Ci.ml^{-1}$ [^{35}S]-SO_4. During the last hour of this period, cells were treated with drug or vehicle as appropriate. SLTxB (1 μl, 1 $mg.ml^{-1}$) was added to wells and incubation continued for a time-course (see Figures and legends). Cells were then washed twice with cold PBS and scraped into 1 ml of lysis buffer (50 mM Tris-HCl pH 7.5, 1% Triton X-100) containing protease inhibitor cocktail (Roche). Cell debris was removed by brief centrifugation (1 minute, 14,000 rpm, in a microfuge) and SLTxB chain was immunoprecipitated from the soluble fraction with sheep anti SLTxB and proteinA-Sepharose at 4°C overnight and washed as previously described [3]. Sulfated SLTxB was identified by autoradiography after SDS-PAGE [81] of the immunoprecipitated material.

Casein degradation assays

Human erythrocyte 26S proteasomes (10 nM, Enzo Life Sciences) were pre-incubated in 20 mM Hepes pH 7.6, 4 mM ATP, 10 mM $MgCl_2$, 1 mM DTT containing 20 μM clasto-Lactacystin β-lactone (Merck) or its vehicle DMSO for 30 minutes at 24°C before addition of 5 μM β-casein (Sigma-Aldritch). After incubation (4 h, 37°C), the samples were subjected to SDS-PAGE and immunoblotting. Casein was revealed by sequential incubations of the blot with sheep anti-casein antibodies (Thermo Scientific) and donkey anti-sheep antibodies conjugated to alkaline phosphatase (Sigma Aldrich) followed by development with BCIP/NBT colour development substrate (Promega).

Supporting Information

Figure S1 Effect of ES_I on subcellular morphology. HeLa cells were treated with 8 μM ES_{R35} or ES_I, or left untreated (UT) for 8 h, then fixed with methanol. Different subcellular compartments were visualised by labelling with anti-PDI (ER), anti-LAMP1 (lysosomes) or anti-Golgin 84 (Golgi appuratus), followed by fluorescently labelled secondary antibodies.
(TIF)

Acknowledgments

Thanks to Martin Lowe for assistance with the VSV-G trafficking assay, and Martin Pool for critical discussions.

Author Contributions

Conceived and designed the experiments: RAS ES SH. Performed the experiments: M-OA CM VP PP RAS. Analyzed the data: RAS SH ES JML. Wrote the paper: RAS ES SH. Designed and directed compound synthesis: RW SLF. Synthesised the drugs used: HW.

References

1. Spooner RA, Smith DC, Easton AJ, Roberts LM, Lord JM (2006) Retrograde transport pathways utilised by viruses and protein toxins. Virol J 3: 26.
2. Bellisola G, Fracasso G, Ippoliti R, Menestrina G, Rosen A, et al. (2004) Reductive activation of ricin and ricin A-chain immunotoxins by protein disulfide isomerase and thioredoxin reductase. Biochem Pharmacol 67: 1721–1731.
3. Spooner RA, Watson PD, Marsden CJ, Smith DC, Moore KA, et al. (2004) Protein disulphide-isomerase reduces ricin to its A and B chains in the endoplasmic reticulum. Biochem J 383: 285–293.
4. Mayerhofer PU, Cook JP, Wahlman J, Pinheiro TT, Moore KA, et al. (2009) Ricin A chain insertion into endoplasmic reticulum membranes is triggered by a temperature increase to 37°C. J Biol Chem 284: 10232–10242.
5. Ye Y, Shibata Y, Yun C, Ron D, Rapoport TA (2004) A membrane protein complex mediates retro-translocation from the ER lumen into the cytosol. Nature 429: 841–847.
6. Sun F, Zhang R, Gong X, Geng X, Drain PF, et al. (2006) Derlin-1 promotes the efficient degradation of the cystic fibrosis transmembrane conductance regulator (CFTR) and CFTR folding mutants. J Biol Chem 281: 36856–36863.
7. Tsai YC, Weissman AM (2010) The Unfolded Protein Response, Degradation from Endoplasmic Reticulum and Cancer. Genes Cancer 1: 764–778.
8. Rabinovich E, Kerem A, Frohlich KU, Diamant N, Bar-Nun S (2002) AAA-ATPase p97/Cdc48p, a cytosolic chaperone required for endoplasmic reticulum-associated protein degradation. Mol Cell Biol 22: 626–634.
9. Elkabetz Y, Shapira I, Rabinovich E, Bar-Nun S (2004) Distinct steps in dislocation of luminal endoplasmic reticulum-associated degradation substrates: roles of endoplamic reticulum-bound p97/Cdc48p and proteasome. J Biol Chem 279: 3980–3989.
10. Ye Y, Meyer HH, Rapoport TA (2001) The AAA ATPase Cdc48/p97 and its partners transport proteins from the ER into the cytosol. Nature 414: 652–656.
11. Stirling CJ, Lord JM (2006) Quality control: linking retrotranslocation and degradation. Curr Biol 16: R1035–1037.
12. Wang Q, Li L, Ye Y (2006) Regulation of retrotranslocation by p97-associated deubiquitinating enzyme ataxin-3. J Cell Biol 174: 963–971.
13. Zhong X, Pittman RN (2006) Ataxin-3 binds VCP/p97 and regulates retrotranslocation of ERAD substrates. Hum Mol Genet 15: 2409–2420.
14. Medicherla B, Kostova Z, Schaefer A, Wolf DH (2004) A genomic screen identifies Dsk2p and Rad23p as essential components of ER-associated degradation. EMBO Rep 5: 692–697.
15. Wesche J, Rapak A, Olsnes S (1999) Dependence of ricin toxicity on translocation of the toxin A-chain from the endoplasmic reticulum to the cytosol. J Biol Chem 274: 34443–34449.
16. Willer M, Forte GM, Stirling CJ (2008) Sec61p is required for ERAD-L: genetic dissection of the translocation and ERAD-L functions of Sec61P using novel derivatives of CPY. J Biol Chem 283: 33883–33888.
17. Slominska-Wojewodzka M, Gregers TF, Walchli S, Sandvig K (2006) EDEM is involved in retrotranslocation of ricin from the endoplasmic reticulum to the cytosol. Mol Biol Cell 17: 1664–1675.
18. Redmann V, Oresic K, Tortorella LL, Cook JP, Lord M, et al. (2011) Dislocation of ricin toxin A chains in human cells utilizes selective cellular factors. J Biol Chem 286: 21231–21238.
19. Spooner RA, Hart PJ, Cook JP, Pietroni P, Rogon C, et al. (2008) Cytosolic chaperones influence the fate of a toxin dislocated from the endoplasmic reticulum. Proc Natl Acad Sci U S A 105: 17408–17413.
20. Endo Y, Tsurugi K (1987) RNA N-glycosidase activity of ricin A-chain. Mechanism of action of the toxic lectin ricin on eukaryotic ribosomes. J Biol Chem 262: 8128–8130.
21. Li S, Spooner RA, Allen SC, Guise CP, Ladds G, et al. (2010) Folding-competent and folding-defective forms of ricin A chain have different fates after retrotranslocation from the endoplasmic reticulum. Mol Biol Cell 21: 2543–2554.
22. Endo Y, Tsurugi K, Yutsudo T, Takeda Y, Ogasawara T, et al. (1988) Site of action of a Vero toxin (VT2) from Escherichia coli O157:H7 and of Shiga toxin on eukaryotic ribosomes. RNA N-glycosidase activity of the toxins. Eur J Biochem 171: 45–50.
23. Yu M, Haslam DB (2005) Shiga toxin is transported from the endoplasmic reticulum following interaction with the luminal chaperone HEDJ/ERdj3. Infect Immun 73: 2524–2532.
24. Falguieres T, Johannes L (2006) Shiga toxin B-subunit binds to the chaperone BiP and the nucleolar protein B23. Biol Cell 98: 125–134.
25. Williams DB, Watts TH (1995) Molecular chaperones in antigen presentation. Curr Opin Immunol 7: 77–84.
26. Cresswell P (2000) Intracellular surveillance: controlling the assembly of MHC class I-peptide complexes. Traffic 1: 301–305.
27. Tortorella D, Gewurz BE, Furman MH, Schust DJ, Ploegh HL (2000) Viral subversion of the immune system. Annu Rev Immunol 18: 861–926.
28. Wiertz EJ, Jones TR, Sun L, Bogyo M, Geuze HJ, et al. (1996) The human cytomegalovirus US11 gene product dislocates MHC class I heavy chains from the endoplasmic reticulum to the cytosol. Cell 84: 769–779.
29. Mueller B, Lilley BN, Ploegh HL (2006) SEL1L, the homologue of yeast Hrd3p, is involved in protein dislocation from the mammalian ER. J Cell Biol 175: 261–270.
30. Mueller B, Klemm EJ, Spooner E, Claessen JH, Ploegh HL (2008) SEL1L nucleates a protein complex required for dislocation of misfolded glycoproteins. Proc Natl Acad Sci U S A 105: 12325–12330.
31. Baker BM, Tortorella D (2007) Dislocation of an endoplasmic reticulum membrane glycoprotein involves the formation of partially dislocated ubiquitinated polypeptides. J Biol Chem 282: 26845–26856.
32. Schulze A, Standera S, Buerger E, Kikkert M, van Voorden S, et al. (2005) The ubiquitin-domain protein HERP forms a complex with components of the endoplasmic reticulum associated degradation pathway. J Mol Biol 354: 1021–1027.
33. Burr ML, Cano F, Svobodova S, Boyle LH, Boname JM, et al. (2011) HRD1 and UBE2J1 target misfolded MHC class I heavy chains for endoplasmic reticulum-associated degradation. Proc Natl Acad Sci U S A 108: 2034–2039.
34. Fiebiger E, Hirsch C, Vyas JM, Gordon E, Ploegh HL, et al. (2004) Dissection of the dislocation pathway for type I membrane proteins with a new small molecule inhibitor, eeyarestatin. Mol Biol Cell 15: 1635–1646.
35. Wang Q, Li L, Ye Y (2008) Inhibition of p97-dependent protein degradation by Eeyarestatin I. J Biol Chem 283: 7445–7454.
36. Wang Q, Shinkre BA, Lee JG, Weniger MA, Liu Y, et al. (2010) The ERAD inhibitor Eeyarestatin I is a bifunctional compound with a membrane-binding domain and a p97/VCP inhibitory group. PLoS One 5: e15479.
37. Dolan BP, Li L, Veltri CA, Ireland CM, Bennink JR, et al. (2011) Distinct pathways generate peptides from defective ribosomal products for CD8+ T cell immunosurveillance. J Immunol 186: 2065–2072.
38. Cross BC, McKibbin C, Callan AC, Roboti P, Piacenti M, et al. (2009) Eeyarestatin I inhibits Sec61-mediated protein translocation at the endoplasmic reticulum. J Cell Sci 122: 4393–4400.
39. Ernst R, Claessen JHL, Mueller B, Sanyal S, Spooner E, et al. (2011) Enzymatic blockade of the ubiquitin-proteasome pathway. PLoS Biol 8: e10000605.
40. Craiu A, Gaczynska M, Akopian T, Gramm CF, Fenteany G, et al. (1997) Lactacystin and clasto-lactacystin beta-lactone modify multiple proteasome beta-subunits and inhibit intracellular protein degradation and major histocompatibility complex class I antigen presentation. J Biol Chem 272: 13437–13445.
41. Tam PJ, Lingwood CA (2007) Membrane cytosolic translocation of verotoxin A1 subunit in target cells. Microbiology 153: 2700–2710.
42. Hudson TH, Neville DM, Jr. (1987) Temporal separation of protein toxin translocation from processing events. J Biol Chem 262: 16484–16494.
43. Neville DM, Jr., Youle RJ (1982) Monoclonal antibody-ricin or ricin A chain hybrids: kinetic analysis of cell killing for tumor therapy. Immunol Rev 62: 75–91.
44. Sandvig K, Ryd M, Garred O, Schweda E, Holm PK, et al. (1994) Retrograde transport from the Golgi complex to the ER of both Shiga toxin and the nontoxic Shiga B-fragment is regulated by butyric acid and cAMP. J Cell Biol 126: 53–64.
45. Sandvig K, Garred O, Prydz K, Kozlov JV, Hansen SH, et al. (1992) Retrograde transport of endocytosed Shiga toxin to the endoplasmic reticulum. Nature 358: 510–512.
46. Mallard F, Antony C, Tenza D, Salamero J, Goud B, et al. (1998) Direct pathway from early/recycling endosomes to the Golgi apparatus revealed through the study of shiga toxin B-fragment transport. J Cell Biol 143: 973–990.
47. Spooner RA, Watson P, Smith DC, Boal F, Amessou M, et al. (2008) The secretion inhibitor Exo2 perturbs trafficking of Shiga toxin between endosomes and the trans-Golgi network. Biochem J 414: 471–484.
48. Blewitt MG, Chung LA, London E (1985) Effect of pH on the conformation of diphtheria toxin and its implications for membrane penetration. Biochemistry 24: 5458–5464.
49. Gallione CJ, Rose JK (1985) A single amino acid substitution in a hydrophobic domain causes temperature-sensitive cell-surface transport of a mutant viral glycoprotein. J Virol 54: 374–382.
50. Presley JF, Cole NB, Schroer TA, Hirschberg K, Zaal KJ, et al. (1997) ER-to-Golgi transport visualized in living cells. Nature 389: 81–85.
51. Hammond C, Helenius A (1994) Quality control in the secretory pathway: retention of a misfolded viral membrane glycoprotein involves cycling between the ER, intermediate compartment, and Golgi apparatus. J Cell Biol 126: 41–52.

52. Donaldson JG, Lippincott-Schwartz J, Bloom GS, Kreis TE, Klausner RD (1990) Dissociation of a 110-kD peripheral membrane protein from the Golgi apparatus is an early event in brefeldin A action. J Cell Biol 111: 2295–2306.
53. Orci L, Tagaya M, Amherdt M, Perrelet A, Donaldson JG, et al. (1991) Brefeldin A, a drug that blocks secretion, prevents the assembly of non-clathrin-coated buds on Golgi cisternae. Cell 64: 1183–1195.
54. Lippincott-Schwartz J, Yuan LC, Bonifacino JS, Klausner RD (1989) Rapid redistribution of Golgi proteins into the ER in cells treated with brefeldin A: evidence for membrane cycling from Golgi to ER. Cell 56: 801–813.
55. Chen SS, Huang AS (1986) Further characterization of the vesicular stomatitis virus temperature-sensitive O45 mutant: intracellular conversion of the glycoprotein to a soluble form. J Virol 59: 210–215.
56. Scheel J, Pepperkok R, Lowe M, Griffiths G, Kreis TE (1997) Dissociation of coatomer from membranes is required for brefeldin A-induced transfer of Golgi enzymes to the endoplasmic reticulum. J Cell Biol 137: 319–333.
57. Wang Q, Mora-Jensen H, Weniger MA, Perez-Galan P, Wolford C, et al. (2009) ERAD inhibitors integrate ER stress with an epigenetic mechanism to activate BH3-only protein NOXA in cancer cells. Proc Natl Acad Sci U S A 106: 2200–2205.
58. Kar R, Singha PK, Venkatachalam MA, Saikumar P (2009) A novel role for MAP1 LC3 in nonautophagic cytoplasmic vacuolation death of cancer cells. Oncogene 28: 2556–2568.
59. White J, Johannes L, Mallard F, Girod A, Grill S, et al. (1999) Rab6 coordinates a novel Golgi to ER retrograde transport pathway in live cells. J Cell Biol 147: 743–760.
60. Monier S, Jollivet F, Janoueix-Lerosey I, Johannes L, Goud B (2002) Characterization of novel Rab6-interacting proteins involved in endosome-to-TGN transport. Traffic 3: 289–297.
61. Del Nery E, Miserey-Lenkei S, Falguieres T, Nizak C, Johannes L, et al. (2006) Rab6A and Rab6A' GTPases play non-overlapping roles in membrane trafficking. Traffic 7: 394–407.
62. Chen A, AbuJarour RJ, Draper RK (2003) Evidence that the transport of ricin to the cytoplasm is independent of both Rab6A and COPI. J Cell Sci 116: 3503–3510.
63. Amessou M, Fradagrada A, Falguieres T, Lord JM, Smith DC, et al. (2007) Syntaxin 16 and syntaxin 5 are required for efficient retrograde transport of several exogenous and endogenous cargo proteins. J Cell Sci 120: 1457–1468.
64. Skönland SS, Walchli S, Utskarpen A, Wandinger-Ness A, Sandvig K (2007) Phosphoinositide-regulated retrograde transport of ricin: crosstalk between hVps34 and sorting nexins. Traffic 8: 297–309.
65. Dyve AB, Bergan J, Utskarpen A, Sandvig K (2009) Sorting nexin 8 regulates endosome-to-Golgi transport. Biochem Biophys Res Commun 390: 109–114.
66. Bujny MV, Popoff V, Johannes L, Cullen PJ (2007) The retromer component sorting nexin-1 is required for efficient retrograde transport of Shiga toxin from early endosome to the trans Golgi network. J Cell Sci 120: 2010–2021.
67. Popoff V, Mardones GA, Bai SK, Chambon V, Tenza D, et al. (2009) Analysis of articulation between clathrin and retromer in retrograde sorting on early endosomes. Traffic 10: 1868–1880.
68. Smith DC, Spooner RA, Watson PD, Murray JL, Hodge TW, et al. (2006) Internalized Pseudomonas exotoxin A can exploit multiple pathways to reach the endoplasmic reticulum. Traffic 7: 379–393.
69. Chadfield MS, Hinton MH (2004) In vitro activity of nitrofuran derivatives on growth and morphology of Salmonella enterica serotype Enteritidis. J Appl Microbiol 96: 1002–1012.
70. Polycarpou-Schwarz M, Muller K, Denger S, Riddell A, Lewis J, et al. (2007) Thanatop: a novel 5-nitrofuran that is a highly active, cell-permeable inhibitor of topoisomerase II. Cancer Res 67: 4451–4458.
71. Maya JD, Bollo S, Nunez-Vergara LJ, Squella JA, Repetto Y, et al. (2003) Trypanosoma cruzi: effect and mode of action of nitroimidazole and nitrofuran derivatives. Biochem Pharmacol 65: 999–1006.
72. Letelier ME, Izquierdo P, Godoy L, Lepe AM, Faundez M (2004) Liver microsomal biotransformation of nitro-aryl drugs: mechanism for potential oxidative stress induction. J Appl Toxicol 24: 519–525.
73. Lakkaraju AK, Luyet PP, Parone P, Falguieres T, Strub K (2007) Inefficient targeting to the endoplasmic reticulum by the signal recognition particle elicits selective defects in post-ER membrane trafficking. Exp Cell Res 313: 834–847.
74. Clague MJ, Urbe S (2006) Endocytosis: the DUB version. Trends Cell Biol 16: 551–559.
75. Wakana Y, Takai S, Nakajima K, Tani K, Yamamoto A, et al. (2008) Bap31 is an itinerant protein that moves between the peripheral endoplasmic reticulum (ER) and a juxtanuclear compartment related to ER-associated Degradation. Mol Biol Cell 19: 1825–1836.
76. Hosokawa N, You Z, Tremblay LO, Nagata K, Herscovics A (2007) Stimulation of ERAD of misfolded null Hong Kong alpha1-antitrypsin by Golgi alpha1,2-mannosidases. Biochem Biophys Res Commun 362: 626–632.
77. Vashist S, Kim W, Belden WJ, Spear ED, Barlowe C, et al. (2001) Distinct retrieval and retention mechanisms are required for the quality control of endoplasmic reticulum protein folding. J Cell Biol 155: 355–368.
78. Fu L, Sztul E (2003) Traffic-independent function of the Sar1p/COPII machinery in proteasomal sorting of the cystic fibrosis transmembrane conductance regulator. J Cell Biol 160: 157–163.
79. Aghi M, Kramm CM, Chou TC, Breakefield XO, Chiocca EA (1998) Synergistic anticancer effects of ganciclovir/thymidine kinase and 5-fluorocytosine/cytosine deaminase gene therapies. J Natl Cancer Inst 90: 370–380.
80. Chiu CF, Ghanekar Y, Frost L, Diao A, Morrison D, et al. (2008) ZFPL1, a novel ring finger protein required for cis-Golgi integrity and efficient ER-to-Golgi transport. Embo J 27: 934–947.
81. Schagger H, von Jagow G (1987) Tricine-sodium dodecyl sulfate-polyacrylamide gel electrophoresis for the separation of proteins in the range from 1 to 100 kDa. Anal Biochem 166: 368–379.